Chapter 5
Broadband Gas QEPAS Detection Exploiting a Monolithic DFB-QCL Array

Marilena Giglio, Andrea Zifarelli, Pietro Patimisco, Angelo Sampaolo, Giansergio Menduni, Arianna Elefante, Romain Blanchard, Christian Pfluegl, Mark F. Witinski, Daryoosh Vakhshoori, Frank K. Tittel, and Vincenzo Spagnolo

Abstract Mid-infrared spectral "fingerprints" of many hazardous and harmful gaseous substances are characterized by broad absorption bands, resulting from the merging of several absorption lines corresponding to ro-vibrational transitions. Broadband absorption spectroscopy is fundamental to detect and discriminate these substances. Here we report on a quartz-enhanced photoacoustic spectroscopy sensor for broadband absorbers detection, employing a monolithic array of 32, individually addressable, distributed-feedback quantum cascade lasers as the excitation source. This light source combines a fast tuning speed with a large tuning range, from 1190 cm^{-1} to 1340 cm^{-1} together with a high stability. The QEPAS sensor was tested for nitrous oxide (N_2O) and methane (CH_4) detection, exhibiting absorption features in the laser source emission spectral range. The two broad P- and R-absorption branches of N_2O have been accurately reconstructed, as well as several absorption features of CH_4, for gas concentrations ranging from 200 to 1000 part-per-million in nitrogen.

Keywords Quartz-enhanced photoacoustic spectroscopy · Gas sensing · Broadband absorbers · Monolithic distributed-feedback quantum cascade laser array · Nitrous oxide · Methane

M. Giglio (✉) · A. Zifarelli · P. Patimisco · A. Sampaolo · G. Menduni · A. Elefante
V. Spagnolo
PolySense Lab – Dipartimento Interateneo di Fisica, University and Politecnico of Bari, CNR – IFN, Bari, Italy
e-mail: marilena.giglio@uniba.it

R. Blanchard · C. Pfluegl · M. F. Witinski · D. Vakhshoori
Pendar Technologies, Cambridge, MA, USA

F. K. Tittel
Department of Electrical and Computer Engineering, Rice University, Houston, TX, USA

M. F. Pereira, A. Apostolakis (eds.), *Terahertz (THz), Mid Infrared (MIR) and Near Infrared (NIR) Technologies for Protection of Critical Infrastructures Against Explosives and CBRN*, NATO Science for Peace and Security Series B: Physics and Biophysics, https://doi.org/10.1007/978-94-024-2082-1_5

5.1 Introduction

Mid-infrared (Mid-IR) and Terahertz (THz) absorption spectra of Chemical Biological Radiological Nuclear (CBRNs) substances and explosive gases are characterized by intense broad bands, in many cases wider than 50 cm^{-1} [1]. An example of broadband absorbers (in gas phase) in the Mid-IR spectral range is shown in Fig. 5.1, where the absorption bands of the main CBRNs are reported, as simulated by using the HITRAN database [2].

At atmospheric pressure, gases like nitrous oxide, carbonyl sulphide, sulphur dioxide, ozone, carbon dioxide, exhibit high spectral density absorption lines in the Mid-IR spectral range, which merge into bands as wide as 100 cm^{-1}, representing a fingerprint for each molecule. Therefore, broadband absorption spectroscopy is fundamental to recognize the presence of such molecules in atmosphere. Moreover, when a gas sample containing many broadband absorber components is analyzed, it is crucial to investigate a spectral region as wide as possible in order to include absorption features belonging to each component, and better discriminate the individual contribution due to each gas species.

For broadband spectroscopy, laser sources tunable in a wide spectral range are required, such as external cavity QCLs (EC-QCLs) or ICLs (EC-ICLs). As a drawback, these devices are quite bulky, may need external liquid cooling systems and suffer from mechanical instability related to the rotating diffraction grating. As a consequence, the spectroscopic technique adopted must rely on a wavelength insensitive detector. In addition, optics components with high performance within a narrow spectral band, such as filters and high reflectivity mirrors, are not

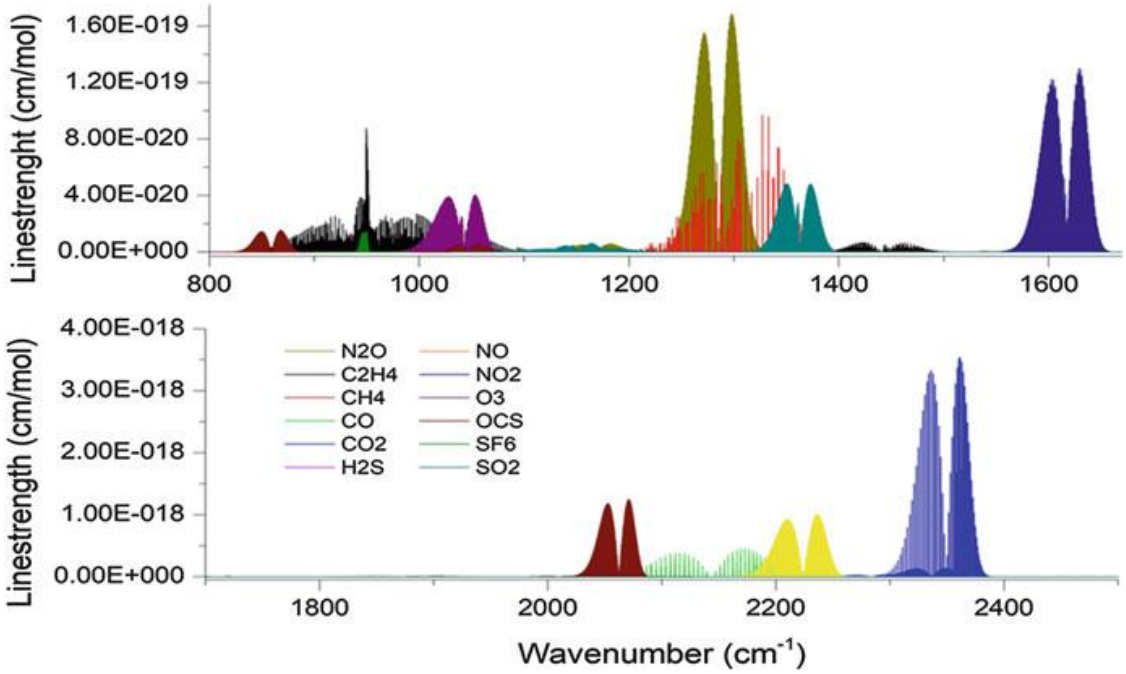

Fig. 5.1 Absorption lines of the main CBRNs and harmful gases in the Mid-IR spectral range simulated by using the HITRAN database

recommended. In this context, Quartz-Enhanced PhotoAcoustic Spectroscopy (QEPAS) can be an excellent candidate for broadband absorption spectroscopy [3–5]. QEPAS consists in exciting the target gas with a laser source whose emission wavelength matches an absorption line or band of the gas. The exciting radiation is modulated in order to generate sound waves, which are detected by a quartz tuning fork (QTF). The radiation is focused between the prongs of the QTF. When the light modulation matches the frequency of a natural flexural vibration of the QTF, electric charges appear on the QTF surface due to the piezoelectric effect. The current signal is proportional to the optical power exciting the gas molecules, the gas absorption coefficient, the QTF quality factor and acousto-electric transduction efficiency [6]. Therefore, QEPAS does not need of an optical detector, whose responsivity is wavelength-dependent. Indeed, QEPAS detection of broadband absorbing molecules has been demonstrated using a widely tunable EC-QCL [7]. In this work, we employed a monolithic distributed-feedback quantum cascade laser array as the light source for a QEPAS sensor, which combines fast tuning speed over a wide spectral range with high stability [8–10]. In addition, the source operates in pulsed mode, suitable for low-power consumption optical sensors technology. This QEPAS sensor has been tested for nitrous oxide (N_2O) and methane (CH_4) detection in the 1190 cm^{-1}–1340 cm^{-1} spectral range, at atmospheric pressure.

5.2 Experimental Setup

The experimental setup used in this work is shown in Fig. 5.2. The employed laser source is an array of 32 individually addressable pulsed DFB-QCLs, powered by a FPGA-based driver capable to control both the injection current and the thermoelectric cooling (TEC). The beams of the different QCLs are spatially overlapped by means of beam combining optics placed inside the laser housing [11]. Emitted beams are spatially filtered using a pinhole and then focused between the prongs of a QTF by an antireflection-coated ZnSe lens with focal length $f = 50$ mm. The QTF is acoustically coupled with a pair of micro-resonator tubes, forming the QEPAS spectrophone, to amplify the sound waves generated by the absorbing gas. The spectrophone is placed inside an acoustic detection module (ADM), consisting in a stainless-steel vacuum-tight cell equipped with two antireflection-coated ZnSe windows and two connectors for gas inlet and outlet. Transmitted power through the ADM is monitored by a power meter.

The laser driver and temperature controller unit are controlled by a LabVIEW-based software and the pulses repetition frequency is triggered by a waveform generator (Wavetek Model 29) to match the QTF resonance frequency f_0. The electric current produced by the QTF is collected and converted into a voltage signal by a transimpedance pre-amplifier (feedback resistance $R_{fb} = 10$ MΩ). This signal is demodulated by a lock-in amplifier (EG&G Instrument 7265) at the reference signal f_0, with an integration time of 100 ms. The analog output signal of the lock-in amplifier is sent to an USB data acquisition device (National Instrument myDAQ) to

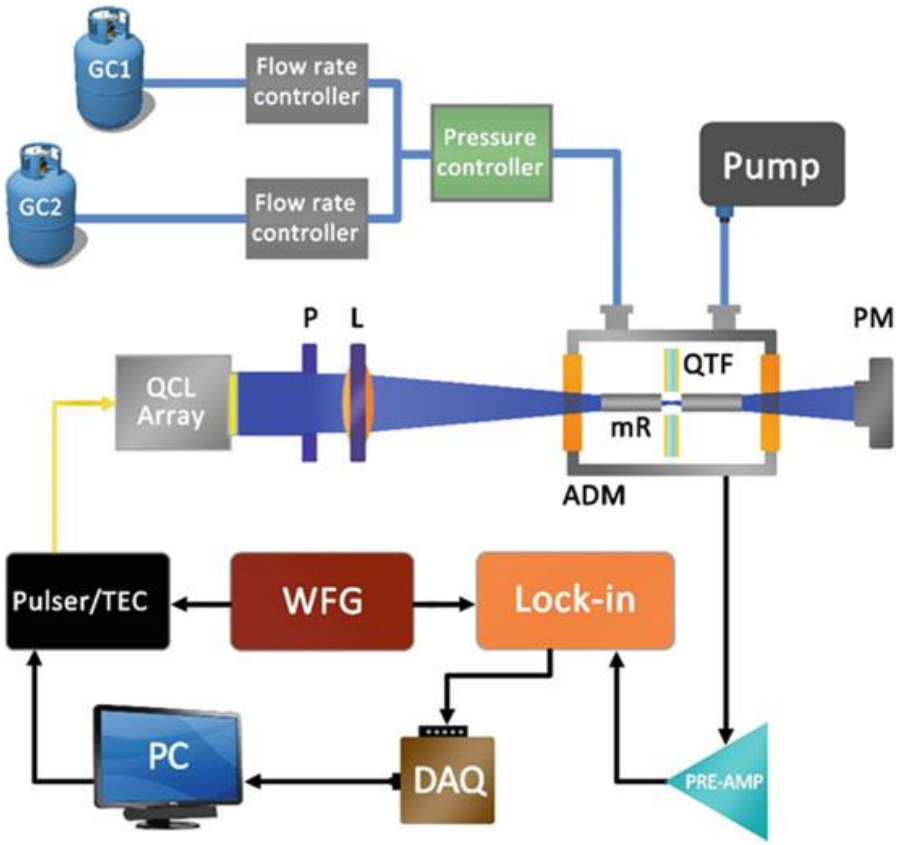

Fig. 5.2 Schematic of the experimental setup. Black lines indicate electrical connections, while blue lines mimic the gas tubes. The golden line indicates the array of cables used to drive the laser source. *GC* Gas Cylinder, *QCL Array* Quantum Cascade Laser array, *P* Pinhole, *L* Lens, *ADM* Acoustic Detection Module, *mR* Micro Resonator tubes, *QTF* Quartz Tuning Fork, *PM* Power Meter, *TEC* Temperature Controller unit, *WFG* Waveform Generator, *PRE-AMP* Pre-amplifier, *DAQ* Data Acquisition board, *PC* Personal Computer

be converted into a digital signal and recorded on the PC using a LabVIEW-based software. The target gas is pumped into the gas line by means of a rotative pump (Adixen Pascal 2021D). Gas flow inside ADM is controlled using flow rate controllers (Brooks Instruments) and a pressure controller (MKS type 649). Flow rate and pressure operation conditions were set at 30 sccm and 760 Torr, respectively.

5.3 Laser Source Characterization and Sensor Configuration

The QCLs comprising the monolithic array are operated in pulsed mode, with a maximum duty cycle of 1%. The devices can be turned on and off in arbitrary sequences. All measurements were performed setting the drive voltage providing the highest optical power output, a pulsewidth of 300 ns and a repetition frequency of 33 kHz (duty cycle of $\approx$ 1%). The spectral emission of the DFB-QCL array was

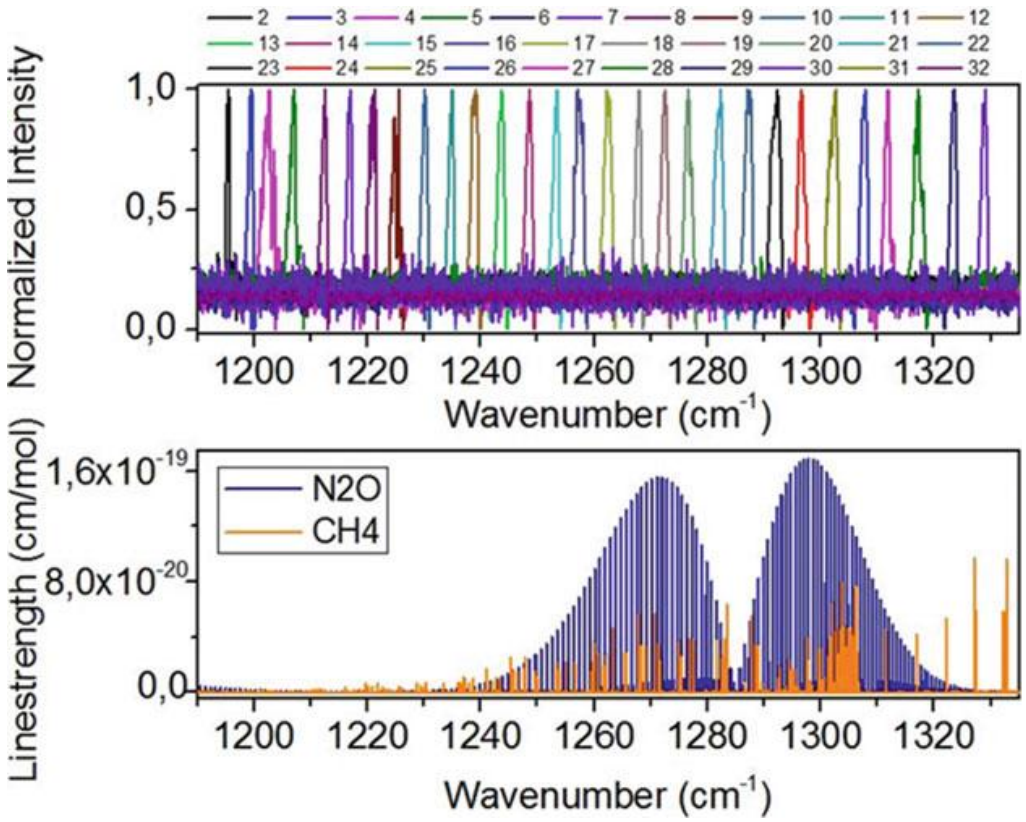

Fig. 5.3 (Upper panel) Normalized spectra of the QCL array acquired by an FTIR. (Lower panel) N_2O and CH_4 absorption lines falling in the QCL array emission spectral range

analysed using a Fourier-transform interferometer (FTIR - Thermo Nicolet 470), with a spectral resolution of 0.125 cm^{-1}. Laser beams exhibit single mode emissions with spectral linewidth of about 1.5 cm^{-1}. As shown in the upper panel of Fig. 5.3, the spectral emission of the array ranges from 1190 cm^{-1} to 1340 cm^{-1}, with a gap between adjacent laser emissions <5 cm^{-1}. In this spectral range, absorption lines of N_2O and CH_4 occur, as shown in the lower panel of Fig. 5.3.

The center emission of each QCL can be tuned by varying the operating temperature. A tuning coefficient of about -0.09 $cm^{-1}/°C$ was measured for each device.

The analysis of the beam profiles was performed by using a pyroelectric-camera (Spiricon Pyrocam III) with pixel size of 100 µm×100 µm, placed in the focal plane of the lens. Figure 5.4a, b show the center position (black squares) and the beam diameter (black solid bars) of each device of the array in *x*- and *y*-direction, respectively.

Within the camera resolution, no shift was observed along the *x*-direction, while a 200 µm shift was observed along the *y*-direction. This allows the estimation of an overall focusing area measuring ~ 600 µm in the *x*-direction and ~ 800 µm in the *y*-direction in order to take into account all shifts related to different devices. Based on these measurements, a 1 mm-prong spacing custom QTF was used in this work,

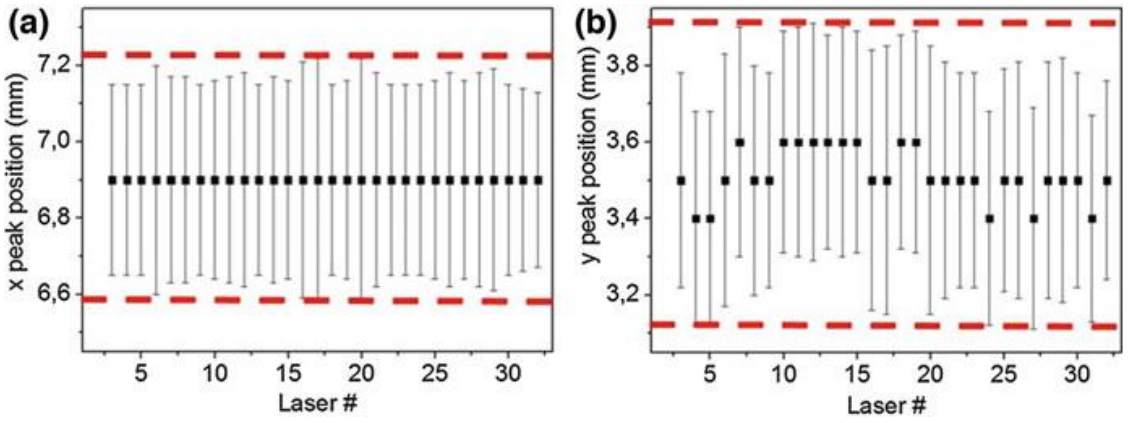

Fig. 5.4 Center position (black squares) and diameter (black solid bars) of the beam profile for each QCL comprising the array. The beam profiles were acquired in the lens focal plane, in x- (**a**) and y- (**b**) direction. Red dashed lines indicate the size of the beam focusing overall region in both directions

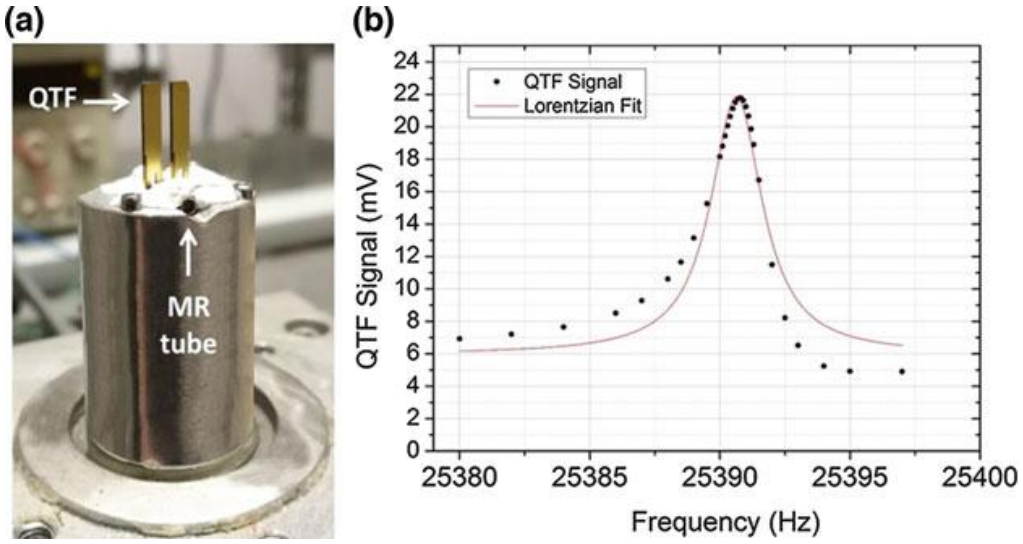

Fig. 5.5 Spectrophone picture (**a**) and electrical characterization at atmospheric pressure (**b**)

having a prong length of 19 mm, a prong width of 1.4 mm and a crystal thickness of 0.8 mm. The QTF was operated at the first overtone flexural mode [12]. Two micro resonator tubes, with internal diameter of 1.52 mm and length of 5.33 mm, were used to amplify the intensity of the photoacoustic waves [12]. A picture of the spectrophone is shown in Fig. 5.4a.

The spectrophone was electrically characterized to determine its resonance frequency and quality factor Q. The obtained resonance curve is shown in Fig. 5.5b as well as the Lorentzian fit. First overtone resonance frequency calculated by the fit is $f_0 = 25390.6$ Hz while quality factor is $Q = 10{,}550$.

5.4 Broadband Absorbers Detection and Sensor Performance

As shown in Fig. 5.3, nitrous oxide and methane show broadband absorption features in the emission spectral range of the employed source. A gas cylinder with a certified concentration of 10,000 part-per-million (ppm) of N_2O in N_2 and a gas cylinder with a certified concentration 1000 ppm of CH_4 in N_2 were used in this work. A cylinder of pure nitrogen was used for further dilutions. Photoacoustic signal generated by the absorbing target gas inside the ADM was collected using two different acquisition modes. The first mode (fixed-temperature mode) consisted in a fast-switching acquisition performed by setting the temperature of the QCLs at 25°C and switching the devices in sequence. Total acquisition time is about 8 min. Spectral resolution is given by the wavenumber distance between two adjacent devices (about 5 cm^{-1}). The second mode (temperature-tuning mode) was performed by tuning the operating temperature of each QCL and switching the devices in sequence. Temperature tuning is performed from 15°C to 50°C, with steps of 3°C, corresponding to a spectral resolution of 0.27 cm^{-1}, resulting in a total measurement time of about 120 minutes.

5.4.1 Nitrous Oxide Detection and Spectrum Reconstruction

The QEPAS signal for a N_2O:N_2 concentration of 1000 ppm, scaled to the QCLs normalized optical power curve of the array, is shown in Fig. 5.6a. Measurements performed in fixed-temperature mode (orange squares) and temperature-tuning mode (blue solid line and dots) are both showed and compared with the HITRAN

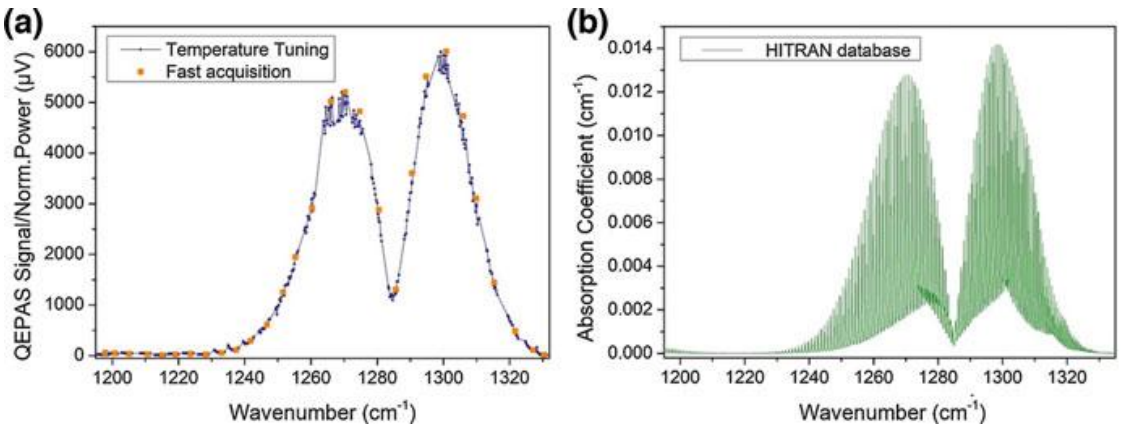

Fig. 5.6 (**a**) QEPAS signals scaled to the normalized optical power as a function of the QCLs wavenumber, for a N_2O:N_2 concentration of 1000 ppm, in fast-switching (orange squares) and temperature tuning (blue solid line and dots) acquisition mode. (**b**) Absorption spectrum of 1000 ppm of N_2O in N_2, simulated using HITRAN database at atmospheric pressure

database-simulation of the N_2O absorption spectrum related to the same concentration [2], reported in Fig. 5.6b.

Measurements acquired in the fast switching acquisition mode overlap the ones obtained in the temperature tuning mode, reducing the acquisition time but worsening the overall spectral resolution of the band reconstruction. Compared with HITRAN simulation, the collected QEPAS measurements trace the envelope of the nitrous oxide absorption spectrum with an excellent matching, both for the fast acquisition and for the temperature tuning acquisition mode. Experimental data well reconstruct the N_2O P- and R- branches, centered at 1270 cm^{-1} and 1298 cm^{-1}. Spectral features of N_2O are well recognizable by using both modes [13]. The certified concentration of nitrous oxide was subsequently diluted in pure nitrogen to test the sensor linearity. QEPAS spectra of 800 ppm, 600 ppm, 400 ppm and 200 ppm N_2O:N_2 were acquired. The QEPAS signal of the acquired spectra linearly scales with the N_2O concentration while the shape was preserved. In particular, the maximum QEPAS signal, which occurs in correspondence of the device emitting at 1274.5 cm^{-1}, was calculated to vary with a slope of 5 μV/ppm.

5.4.2 *Methane Detection and Spectrum Reconstruction*

Methane measurements were performed using the same procedure followed for nitrous oxide. Figure 5.7a shows the QEPAS signal scaled to the normalized optical power of each device of the array, for a certified CH_4:N_2 concentration of 1000 ppm. Measurements obtained with fixed-temperature (orange squares) and temperature-tuning (blue solid line and dots) acquisition modes are reported. As a comparison, the absorption spectrum of the same concentration of CH_4:N_2 simulated by using the HITRAN database at atmospheric pressure is reported in Fig. 5.7b.

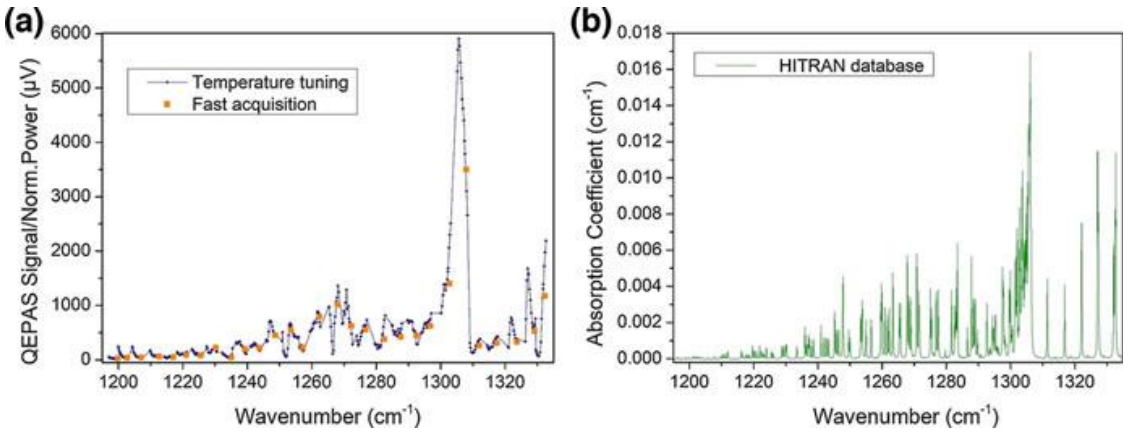

Fig. 5.7 (**a**) QEPAS signals scaled to the normalized optical power as a function of the QCLs wavenumber, for a CH_4:N_2 concentration of 1000 ppm, in fast-switching (orange squares) and temperature tuning (blue solid line and dots) acquisition mode. (**b**) Absorption spectrum of 1000 ppm of CH_4 in N_2, simulated using HITRAN database at atmospheric pressure

Measurements acquired in the fast switching acquisition mode overlap the ones obtained in the temperature tuning mode and the absorption peak at 1306.13 cm^{-1}, corresponding to the Q-branch of the methane ro-vibrational transitions, is well traced by both acquisition modes. However, lower intensity peaks are less distinguishable. A linear response of the QEPAS sensor for methane detection was demonstrated by diluting the certified concentration of methane in pure nitrogen. The maximum QEPAS signal of the methane spectrum, which occurs in correspondence of the device emitting at 1306 cm^{-1}, was calculated to vary with the methane concentration with a slope of 2 μV/ppm [14].

5.5 Conclusion

In this work, broadband detection of nitrous oxide and methane was demonstrated by using QEPAS-based sensor employing a monolithic array composed of 32 individually addressable distributed feedback-quantum cascade lasers as the light source. Within the laser source emission spectral range, from 1190 cm^{-1} to 1340 cm^{-1}, the two broad P- and R- absorption branches of nitrous oxide were reconstructed, as well as the Q-branch of methane. Two acquisition modes were tested, a fast-switching of individual devices in sequence, fixing the operation temperature at 25°C for each device, and higher resolution mode, tuning the operating temperature of each device together with the device switching in series. Sensor linearity for gases concentration in the 1000 ppm–200 ppm range was also demonstrated, both for methane and nitrous oxide.

Acknowledgments The authors from Dipartimento Interateneo di Fisica di Bari acknowledge financial support from THORLABS GmbH, within the joint-research laboratory PolySense. Frank K. Tittel acknowledges support by the Welch Foundation (Grant C0568). Pendar Technologies acknowledges support from the US Army (W911SR-16-C-0005).

References

1. Herzberg G (2016) Molecular spectra and molecular structure, vol 1. Read Books, New York
2. http://hitran.org/
3. Sampaolo A, Csutak S, Patimisco P, Giglio M, Menduni G, Passaro V, Tittel FK, Deffenbaugh M, Spagnolo V (2019) Methane, ethane and propane detection using a compact quartz enhanced photoacoustic sensors and a single interband cascade laser. Sens Act B Chem 282:952–960
4. Giglio M, Elefante A, Patimisco P, Sampaolo A, Sgobba F, Rossmadl H, Mackowiak V, Wu H, Tittel FK, Dong L, Spagnolo V (2019) Quartz-enhanced photoacoustic sensor for ethylene detection implementing optimized custom tuning fork-based spectrophone. Opt Express 27(4):4271–4280

5. Sampaolo A, Patimisco P, Giglio M, Chieco L, Scamarcio G, Tittel FK, Spagnolo V (2016) Highly sensitive gas leak detector based on a quartz-enhanced photoacoustic SF6 sensor. Opt Express 24:15872–15881
6. Patimisco P, Sampaolo A, Dong L, Tittel FK, Spagnolo V (2018) Recent advances in quartz enhanced photoacoustic sensing. Appl Phys Rev 5:011106
7. Lewicki R, Wysocki G, Kosterev AA, Tittel FK (2007) QEPAS based detection of broadband absorbing molecules using a widely tunable, cw quantum cascade laser at 8.4 μm. Opt Express 15(12):7357–7366
8. Lee BG, Belkin MA, Pflugl C, Diehl L, Zhang HA, Audet RM, MacArthur J, Bour DP, Corzine SW, Hofler GE, Capasso F (2009) DFB quantum cascade laser arrays. IEEE J Quantum Electron 45:554–565
9. Witinski MF, Blanchard R, Pfluegl C, Diehl L, Li B, Krishnamurthy K, Pein BC, Azimi M, Chen P, Ulu G et al (2018) Portable standoff spectrometer for hazard identification using integrated quantum cascade laser arrays from 6.5 to 11 μm. Opt Express 26:12159
10. Lee BG, Belkin MA, Audet R, MacArthur J, Diehl L, Pflügl C, Capasso F, Oakley DC, Chapman D, Napoleone A et al (2007) Widely tunable single-mode quantum cascade laser source for mid-infrared spectroscopy. Appl Phys Lett 91:231101
11. Lee BG, Kansky J, Goyal AK, Pflügl C, Diehl L, Belkin MA, Sanchez A, Capasso F (2009) Beam combining of quantum cascade laser arrays. Opt Express 17:16216
12. Patimisco P, Sampaolo A, Zheng H, Dong L, Tittel FK, Spagnolo V (2016) Quartz enhanced photoacoustic spectrophones exploiting custom tuning forks: a review. Adv Phys X 2:169–187
13. Giglio M, Patimisco P, Sampaolo A, Zifarelli A, Blanchard R, Pfluegl C, Witinski MF, Vakhshoori D, Tittel FK, Spagnolo V (2018) Nitrous oxide quartz-enhanced photoacoustic detection employing a broadband distributed-feedback quantum cascade laser array. Appl Phys Lett 113:171101
14. Giglio M, Zifarelli A, Sampaolo A, Menduni G, Elefante A, Blanchard R, Pfluegl C, Witinski MF, Vakhshoori D, Wu H, Passaro VMN, Patimisco P, Tittel FK, Dong L, Spagnolo V (2020) Broadband detection of methane and nitrous oxide using a distributed-feedback quantum cascade laser array and quartz-enhanced photoacoustic sensing. Photoacoustics 17:100159